Vectorially Oriented Monolayers of Detergent-Solubilized Ca^{2+}-ATPase from Sarcoplasmic Reticulum

Lisa A. Prokop,* Robert M. Strongin,* Amos B. Smith, III,* J. Kent Blasie,* Lawrence J. Peticolas,‡ and John C. Bean‡

*Department of Chemistry, University of Pennsylvania, Philadelphia, Pennsylvania 19104, and ‡AT&T Bell Laboratories, Murray Hill, New Jersey 07974 USA

ABSTRACT A method for tethering proteins to solid surfaces has been utilized to form vectorially oriented monolayers of the detergent-solubilized integral membrane protein Ca^{2+}-ATPase from the sarcoplasmic reticulum (SR). Bifunctional, organic self-assembled monolayers (SAMs) possessing "headgroup" binding specificity for the substrate and "endgroup" binding specificity for the enzyme were utilized to tether the enzyme to the substrate. Specifically, an amine-terminated 11-siloxyundecaneamine SAM was found to bind the Ca^{2+}-ATPase primarily electrostatically. The Ca^{2+}-ATPase was labeled with the fluorescent probe 5-{2-[(iodoacetyl)amino]ethyl}aminonaphthalene-1-sulfonic acid before monolayer formation. Consequently, fluorescence measurements performed on amine-terminated SAM/enzyme monolayers formed on quartz substrates served to establish the nature of protein binding. Formation of the monolayers on inorganic multilayer substrates fabricated by molecular beam epitaxy made it possible to use x-ray interferometry to determine the profile structure for the system, which was proved correct by x-ray holography. The profile structures established the vectorial orientation of the Ca^{2+}-ATPase within these monolayers, to a spatial resolution of ~12 Å. Such vectorially oriented monolayers of detergent-solubilized Ca^{2+}-ATPase from SR make possible a wide variety of correlative structure/function studies, which would serve to elucidate the mechanism of Ca^{2+} transport by this enzyme.

INTRODUCTION

The calcium pump protein of the sarcoplasmic reticulum (SR), Ca^{2+}-ATPase, is a member of the class of integral membrane proteins termed ion-motive ATPases and is responsible for the relaxation phase of the contraction/relaxation cycle in striated and cardiac muscle. This relaxation phase is a result of the active (energy-dependent) transport of calcium ions from the cytoplasm, across the sarcoplasmic reticulum membrane and into the sarcotubular system (Ebashi et al., 1969). This SR Ca^{2+}-ATPase is thus a widely studied enzyme (for reviews see de Meis and Vianna, 1979; Ikemoto, 1982; Inesi, 1985) because of its important role in excitation-contraction coupling. Investigations of the SR Ca^{2+}-ATPase have been facilitated by the ease of isolation of the SR membrane and the high concentration of Ca^{2+}-ATPase that is obtained in purified membrane preparations (~90% of the total protein) (Meissner et al., 1973). These facts have made Ca^{2+}-ATPase a prototypical pump protein for the study of energy-dependent ion transport across biological membranes.

Over the past decade many experiments have been undertaken to correlate the structure of the SR Ca^{2+}-ATPase with its function in an attempt to gain an understanding of its mechanism of Ca^{2+} transport. Coupled x-ray and neutron diffraction studies were significant in establishing the cylindrically averaged profile structure (about the normal to the membrane plane) of Ca^{2+}-ATPase itself within the fully functional isolated SR membrane, and served to establish the "headpiece," "stalk," and "transmembrane" domains of the enzyme (Herbette et al., 1985). This profile structure was found to be consistent with the subsequently described putative secondary and tertiary structure for the enzyme, based on its primary amino acid sequence (MacLennan et al., 1985), as well as the more recently determined moderate-resolution, three-dimensional structure of the enzyme determined by cryo-electron microscopy of tubular crystals of Ca^{2+}-ATPase induced in the isolated SR membranes by vanadate and embedded in amorphous ice (Toyoshima et al., 1993). Time-resolved x-ray diffraction studies on oriented multilayers of isolated SR have established that large-scale (i.e., long-range) structural changes occur throughout the moderate-resolution, cylindrically averaged profile structure of the SR Ca^{2+}-ATPase upon enzyme phosphorylation during Ca^{2+} transport (Blasie et al., 1990). More recently, resonance x-ray diffraction was employed as a means of locating the positions of lanthanide ions (La^{3+} and Tb^{3+}) replacing Ca^{2+} on the metal-binding sites within the profile structure of the resting and phosphorylated forms of the enzyme within the isolated SR membrane (Asturias and Blasie, 1991; Asturias et al., 1994b). However, we still lack a complete understanding of the mechanism of active calcium transport by Ca^{2+}-ATPase, due in part to the lack of an atomic resolution three-dimensional structure for this enzyme, which stems from difficulties in producing either three-dimensional or two-dimensional crystals of detergent-solubilized Ca^{2+}-ATPase with sufficient long-range order

Received for publication 13 October 1995 and in final form 7 February 1996.

Address reprint requests to Dr. Lisa A. Prokop, Department of Chemistry, University of Pennsylvania, 231 S. 34th Street, Philadelphia, PA 19104-6323. Tel.: 215-898-2097; Fax: 215-898-6242; E-mail: prokop@jkb.chem.upenn.edu.

0006-3495/96/05/2131/13 $2.00

suitable for high-resolution x-ray or electron crystallographic structure determination. Ultimately, time-resolved studies of the profile structures of Ca^{2+}-ATPase in oriented SR membrane multilayers describing the active ion transport mechanism must be coupled to such a high-resolution, three-dimensional structure. Ideally, one would like to utilize a single system with Ca^{2+}-ATPase in a form amenable to all of the experiments described above. Thus, we sought to design a system for which time-resolved x-ray diffraction studies of the Ca^{2+}-ATPase structure could be extended, not only to higher resolution in the profile structure, but also from the profile structure toward the full three-dimensional structure of the enzyme. In addition to functional studies of the calcium transport kinetics, the system had to be amenable to neutron and time-resolved resonance x-ray diffraction studies of the sorts described above. Furthermore, it had to be suitable for x-ray or electron crystallographic structure determination of the three-dimensional structure of the Ca^{2+}-ATPase to atomic resolution. As a result, it has been necessary to devise methods for controlling the three-dimensional organization of the integral membrane protein while maintaining the "unidirectional" or vectorial orientation of the protein that is inherent in the native membrane. Maintenance of the vectorial orientation of the protein, or the orientation of that vector representing the internal coordinate of the protein molecule relative to the coordinate frame of the membrane (Chupa et al., 1994), is paramount for structural studies that can be directly correlated with functional characteristics of the enzyme in question.

Recent work (Chupa et al., 1994) has demonstrated the ability to form densely packed, vectorially oriented monolayers of both peripheral and integral membrane proteins on the surfaces of solid substrates suitable for structural characterizations by x-ray diffraction, namely yeast (*Saccharomyces cerevisiae*) cytochrome *c* and photosynthetic reaction centers (*Rhodopseudomonas sphaeroides*). In each case the proteins were reversibly tethered to the surface of Ge/Si multilayer substrates fabricated by molecular beam epitaxy (MBE) via bifunctional, organic self-assembled monolayers (SAMs) possessing a "headgroup" with binding specificity for the substrate and an "endgroup" with binding specificity for the protein. The thinness of the Ge layers (limited in principle to the thickness of a single Ge atomic monolayer of ~3.5 Å) achievable with MBE fabrication enabled the determination of the profile structures for these systems by x-ray interferometry with an improved spatial resolution of ~7 Å, as compared to prior work performed on sputtered Ge/Si multilayer substrates (Amador et al., 1993). This high resolution was sufficient to establish the vectorial orientation of the protein molecules in the monolayers. Because the three-dimensional crystal structures of these two proteins are known to atomic resolution, this work served as a test case for the ability to form vectorially oriented membrane protein monolayers on solid substrates.

This study extends the work described above to Ca^{2+}-ATPase from SR. Fig. 1 shows a schematic representation of the system under investigation, in which Ca^{2+}-ATPase,

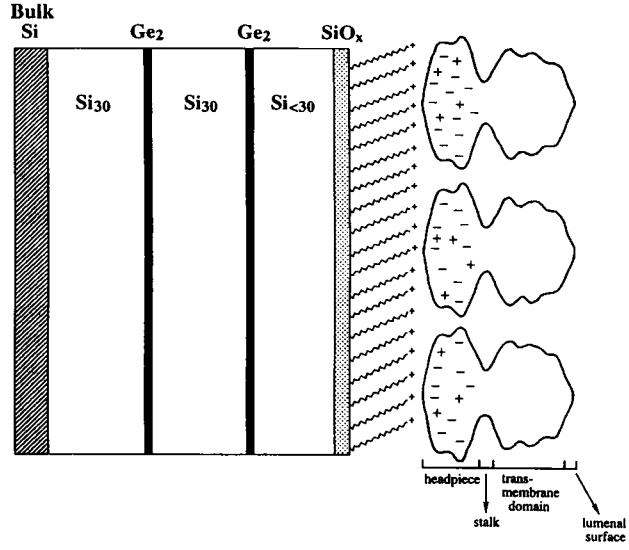

FIGURE 1 Schematic representation of the Ca^{2+}-ATPase electrostatically tethered to the surface of a Ge/Si multilayer substrate via an amine-terminated SAM. The enzyme is shown as a representation of the 11-Å resolution cylindrically averaged profile structure determined previously by combined x-ray and neutron diffraction (Herbette et al., 1985). The domains of the enzyme have been labeled. The charge distribution shown in the "headpiece" of the enzyme is meant to represent a net negative charge in this region. The cylindrical *z* axis is perpendicular to the monolayer plane. The 11-siloxyundecaneamine SAM is represented as a long carbon chain with a positively charged endgroup. The tilt angle of the chains has not been measured in this work, but we feel that such an arbitrary tilt from the normal to the substrate plane best represents the SAM, as demonstrated previously for methyl-terminated chains (Xu et al., 1993).

represented by its previously determined, cylindrically averaged profile structure (Herbette et al., 1985), is electrostatically tethered to the surface of an amine-terminated 11-siloxyundecaneamine SAM, which in turn is covalently bound to the surface of a Ge/Si multilayer substrate. The techniques of x-ray interferometry and x-ray holography were used to establish the profile structure for this system, to a spatial resolution of ~12 Å, which verified the vectorial orientation of Ca^{2+}-ATPase within these monolayers. Comparisons are made between the results of this structural study and earlier studies on Ca^{2+}-ATPase in the isolated SR membrane. The applications of this particular system with regard to further structural and functional studies of SR Ca^{2+}-ATPase will also be discussed.

MATERIALS AND METHODS

Dispersions of SR membrane vesicles were prepared from rabbit hind leg white muscle according to the method of McFarland and Inesi (1971) described previously (Herbette et al., 1977). This "crude SR" preparation was further purified by discontinuous density gradient centrifugation (Watras et al., 1984) as follows. Crude SR was diluted to 10 mg/ml with 10% (w/v) sucrose (ICN Biomedicals, Aurora, OH); loaded onto a discontinuous sucrose gradient composed of 3 ml of 60%, 10 ml of 40%, 10 ml of 31%, and 10 ml of 28% sucrose; and centrifuged at 90,000 × *g* for 4 h

at 4°C in a Beckman SW28 rotor (Beckman Instruments, Palo Alto, CA). Light SR vesicles concentrate at the 28/31% sucrose interface (Meissner, 1975); these were removed from the gradient with a blunt-needle syringe. This light SR preparation was then concentrated and resuspended in a medium containing 100 mM $MgCl_2$ (EM Science, Cherry Hill, NJ), 100 mM KCl, and 2 mM trizma-maleate (Sigma Chemical Co., St. Louis, MO), pH 6.85. We call this preparation "pure SR," which typically contained 14–18 mg protein/ml, of which ~90% is Ca^{2+}-ATPase (Meissner et al., 1973).

Next, membranous Ca^{2+}-ATPase was labeled with the fluorescent probe 5-{2-[(iodoacetyl)amino]ethyl}aminonaphthalene-1-sulfonic acid (1,5-IAEDANS) (Fluka Chemical Corp., Ronkonkoma, NY) according to the method of Squier et al. (1987). This probe reacts covalently with cysteines 670 and 674 on the B tryptic fragment of the enzyme (Bigelow et al., 1992). The Ca^{2+}-ATPase was labeled for 30 min at room temperature in the dark by incubating 4 mg pure SR/ml in a medium containing 20 mM 3-[*N*-morpholino]propane sulfonic acid (MOPS) (Sigma Chemical Co.), pH 6.8, 80 mM KCl, 1 mM $CaCl_2$ (EM Science), 5 mM $MgCl_2$, and excess 1,5-IAEDANS to ensure complete modification of the reactive sulfhydryls on the protein (~70 moles 1,5-IAEDANS:1 mole Ca^{2+}-ATPase). Unreacted 1,5-IAEDANS was removed with a Sephadex G-50 column (Sigma Chemical Co.) followed by centrifugation at 40,000 × *g* for 45 min at 5°C in a Beckman Ti 70.1 rotor. The "labeled pure SR" pellet was resuspended in buffer solution (20 mM MOPS, pH 6.8, 80 mM KCl, 1 mM $CaCl_2$, 5 mM $MgCl_2$), resulting in a suspension whose concentration was typically 7–15 mg protein/ml. Finally, this membranous labeled Ca^{2+}-ATPase was solubilized in the nonionic detergent polyoxyethylene 9 lauryl ether ($C_{12}E_9$) (Sigma Chemical Co.) according to the method of Coll and Murphy (1984). This procedure involved solubilizing the labeled pure SR at a final concentration of 1.5–2.0 mg/ml in a medium containing 20 mg/ml $C_{12}E_9$, 20% sucrose (w/v), 1 mM $CaCl_2$, 1 mM $MgCl_2$, and 50 mM MOPS, pH 7.0, followed by centrifugation at 27,000 × *g* for 30 min at 5°C in a Beckman Ti 70.1 rotor. Protein concentration of the supernatant was typically 2–3 mg/ml at this point in the procedure. The detergent-solubilized Ca^{2+}-ATPase was aliquoted into appropriately sized fractions, frozen in liquid N_2, and stored at −80°C until it was used. Successful labeling was verified by recording the fluorescence emission spectrum of this protein solution diluted to ~0.2 μM, because the emission spectrum of 1,5-IAEDANS-labeled SR is known from the literature (Squier et al., 1987). All solutions described above were prepared with ultrapure water as the solvent (MilliQ water system; Millipore Corp., Bedford, MA). Protein concentration was determined by the method of Lowry et al. (1951) throughout these preparations where indicated, using bovine serum albumin as the standard.

The Ge/Si multilayer substrates used in the x-ray diffraction experiments were fabricated by MBE at AT&T Bell Laboratories (Bean and Sadowski, 1982). The multilayer superlattices were grown on 4-inch p-type Si(100) wafers (SEH-America, Vancouver, WA) with a resistivity of 20 Ω cm. Substrate growth was initiated by depositing 30 atomic monolayers of silicon (Si_{30}) onto the base Si(100) wafer to smooth the surface, followed by deposition of 2 atomic monolayers of germanium (Ge_2) and 30 of silicon (Si_{30}), twice, forming the two-unit-cell superlattice structure of the form $2(Ge_2Si_{30})$. Details of the MBE growth procedures are provided elsewhere (Bean et al., 1984). The superlattice unit cell, (Ge_2Si_{30}), has a profile thickness of ~35.5 Å, which was chosen to roughly coincide with the thickness of the organic/bio-organic overlayers to be formed on the surface of the substrates (Murphy et al., 1993; Xu et al., 1993; Chupa et al., 1994). Matching the thickness of the Ge/Si multilayer to that of the SAM/enzyme overlayers generated strong kinematical x-ray diffraction from the reference Ge/Si multilayer structure over regions of reciprocal space perpendicular to the substrate plane (i.e., along the q_z axis), where x-ray scattering from the overlayer structures is expected to be strong. The use of only two unit cells in the superlattice structures allows for the generation of continuous meridional x-ray diffraction over a broad range of q_z and therefore maximum interference with the scattering from the unknown overlayer structure (Cowley, 1981). Finally, choosing to make the more electron-dense Ge layers in the MBE substrates very thin ensures the generation of more intense x-ray diffraction out to larger q_z, as compared to substrates fabricated by magnetron sputtering described previously (Amador et al., 1993; Xu et al., 1991). The MBE wafers were cut with a diamond pencil to obtain 1 cm × 2 cm × 0.5 mm substrates.

The organic compound 11-*N*-(*tert*-butoxycarbonyl)aminoundecyltriethoxysilane was the precursor for the amine-terminated SAM, and its synthesis has been described in detail previously (Chupa et al., 1994). SAMs were formed on the surfaces of both quartz substrates (10 mm × 20 mm × 1 mm) for fluorescence measurements and the Ge/Si multilayer substrates by the modified method of Sagiv (1980) as described by Xu et al. (1993), with further modifications. These modifications involved eliminating the 5 mM NaOH cleaning step and increasing the alkylation time (i.e., the time that the substrates were sonicated in a solution containing the amine-terminated SAM precursor compound) from 22 to 45 min. These "protected amine" SAMs were then activated by removing the protecting *tert*-butoxycarbonyl groups by acid hydrolysis (immersing the substrates in concentrated HCl for 1.5 h) to form the amine-terminated SAM 11-siloxyundecaneamine. After rinsing in ~4 liters of ultrapure water, the substrates were placed in vials containing 5–8 μM Ca^{2+}-ATPase in 1 mM MOPS buffer at pH 7.0 with 0.1% $C_{12}E_9$, 1 mM $CaCl_2$, and 1 mM $MgCl_2$, and incubated for ~48 h at 4°C.

Fluorescence emission spectra were recorded for the amine SAM/protein samples on quartz substrates to detect the presence of 1,5-IAEDANS-labeled Ca^{2+}-ATPase using a Perkin-Elmer model LS50 luminescence spectrometer (Perkin-Elmer, Beaconsfield, Buckinghamshire, England) interfaced to a Dell 486D/50 computer. The spectrometer possessed the typical geometry used for measuring fluorescence from samples, where the emission monochromator and detection system are situated 90° to the excitation monochromator and light source. The following procedure was developed for measuring fluorescence from single monolayers of Ca^{2+}-ATPase formed on solid substrates. The quartz substrate was removed from its incubating solution and placed in a fluorescence cuvette (optically polished on all sides) containing "detergent buffer" (1 mM MOPS, pH 7.0, 0.1% $C_{12}E_9$, 1 mM $CaCl_2$, 1 mM $MgCl_2$) and was held in a specific orientation by a sample holder that was made to fit inside the bottom of the cuvette, with a slot that was ~23° from the diagonal of the holder and wide enough for the quartz substrate to fit into. This orientation of the substrate ensured that the incident UV excitation beam was intercepted at "grazing incidence," thereby minimizing its reflection into the emission optics. Fluorescence emission spectra were recorded using excitation slits of 4.0 nm and emission slits of 2.5 nm, with the excitation wavelength, λ_{ex}, equal to 340 nm. After this initial fluorescence emission spectrum was recorded, the substrate was removed from the cuvette and placed in a clean vial containing the detergent buffer described above (i.e., low-ionic-strength buffer) for 1 min without agitation, to remove nonspecifically bound protein from the substrate surface. The substrate was then placed back in the cuvette, with fresh detergent buffer, and the fluorescence emission spectrum was recorded again. This procedure was performed until the fluorescence emission signal no longer decreased with successive washings of the substrate, indicating that nonspecifically bound protein had been removed and only the protein molecules specifically bound (see Discussion) to the amine-terminated SAM remained. This procedure was performed as verification of protein binding before collecting meridional x-ray diffraction data from the analogous MBE substrates, with the MBE substrates being "washed" the same number of times as it took to reach the "baseline" fluorescence emission from the quartz substrates to remove nonspecifically bound protein from the samples.

Meridional x-ray diffraction data [$I(q_{xy} = 0$ Å, $q_z)$], which corresponds to elastic photon momentum transfer parallel to the *z* axis perpendicular to the substrate plane, was collected for each Ge/Si multilayer substrate before and after formation of the protected amine SAM and the amine SAM/protein monolayers, as a function of $q_z = (2 \sin \theta)/\lambda$. This meridional x-ray diffraction arises from the projection of the three-dimensional electron density distribution of the multilayer specimen along radial vectors perpendicular to the *z* axis onto the *z* axis; this projection is defined as the electron density profile, $\rho(z)$, for the multilayer specimen. The incident x-ray beam defines an angle (ω) with the substrate plane (xy), with meridional x-ray diffraction being observed for ω equal to θ, where 2θ is the angle between the incident and scattered beams.

The multilayer specimens were positioned on the ϕ axis of a Huber 4-circle diffractometer, which was oscillated over an appropriate range of ω values. This geometry enabled collection of meridional x-ray diffraction data with a two-dimensional, position-sensitive detector (Siemens Instruments, Madison, WI), which was mounted on the 2θ axis and interfaced to a GPXII Micro VAX computer (Digital Equipment Corp., Marlboro, MA). An Elliott GX-13 rotating anode x-ray generator (Enraf-Nonius, Bohemia, NY) operating at a target loading of 27 kW/mm^2 was used to produce the incident Cu emission spectrum. The $CuK_{\alpha 1}$ line (λ = 1.541 Å) was selected with a 37 mm × 20 mm cylindrically bent Ge(111) monochromator crystal (Innovative Technology, South Hamilton, MA) to produce a line-focused x-ray beam parallel to the ω axis. The specimen-to-detector distance was 350 mm, and the beam height was ~6 mm at the specimen. The incident and scattered beams were in a dry helium atmosphere. The focused x-ray beam width at the detector and the spatial resolution of the two-dimensional, position-sensitive detector resulted in a Δq_z resolution of ~0.0009 Å^{-1}. Meridional x-ray diffraction patterns were collected in sequential 35-min time frames over an ~17-h time period and stored as two-dimensional data files. Each two-dimensional data file was integrated perpendicular to the q_z axis over the length of the line-focused x-ray beam, producing a one-dimensional data file (i.e., the number of x-ray counts vs. detector channel number along the q_z axis). These one-dimensional data files were first examined for possible radiation damage or specimen instability over the course of data collection. No evolution of the meridional x-ray diffraction from the specimens over the total data collection time was evident. The two-dimensional data files themselves were then summed and corrected for any detector nonuniformities by employing a correction algorithm based on a two-dimensional data file obtained from uniform illumination of the detector with an ^{55}Fe source. These summed and corrected files were then integrated to produce one-dimensional data files, which were transferred to a Silicon Graphics IRIS Indigo computer (Silicon Graphics, Mountain View, CA) for further analysis (see Results below).

Throughout data collection, the bare Ge/Si multilayer substrates and the protected amine SAMs were housed in an aluminum chamber with saran (polyvinylidene chloride) windows (Goodfellow Corp., Cambridge, England) in a dry helium atmosphere at room temperature (22 ± 0.5°C). The deprotected amine SAM/Ca^{2+}-ATPase specimens were housed in the same specimen chamber and maintained at 3–7°C and a constant relative humidity (94 ± 1%) with a humidity controller (Asturias et al., 1994a). This humidity controller constantly circulated moist helium through the specimen chamber to maintain the hydration of the protein samples.

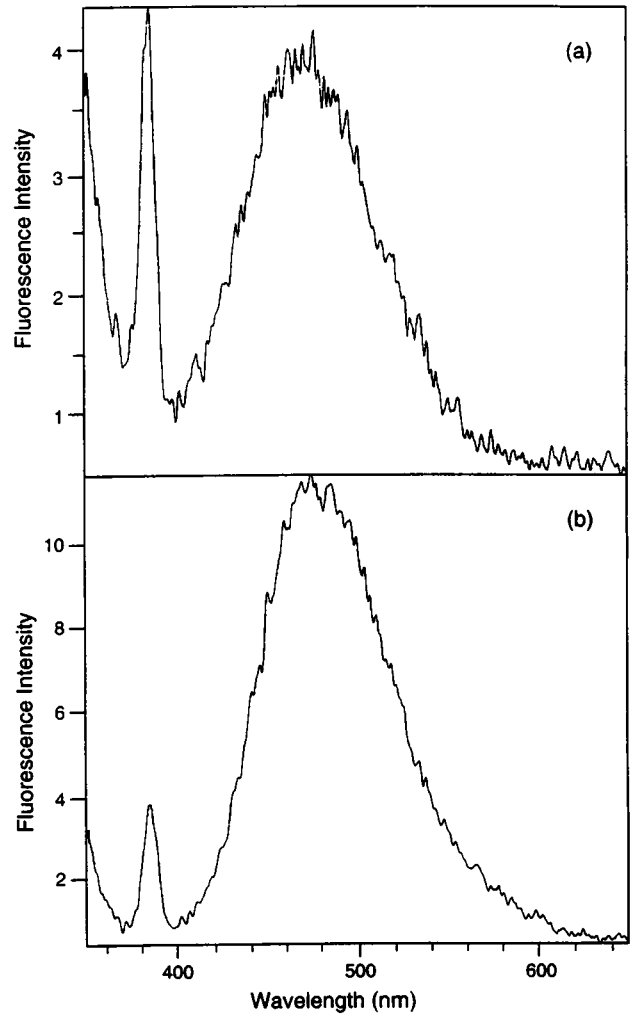

FIGURE 2 (*a*) Fluorescence emission spectrum for detergent-solubilized, 1,5-IAEDANS-labeled Ca^{2+}-ATPase electrostatically tethered to the surface of an 11-siloxyundecaneamine SAM on quartz. The broad emission feature centered at ~476 nm is indicative of the presence of labeled enzyme. The origin of the sharp feature at ~384 nm is the MOPS buffer that was present in the cuvette with the sample to maintain its hydration and pH. (*b*) Fluorescence emission spectrum for pure SR vesicles electrostatically tethered to the surface of an 11-siloxyundecaneamine SAM on quartz, in which the Ca^{2+}-ATPase within the SR membrane has been labeled with 1,5-IAEDANS. The emission maximum is ~2 times as intense as that in (*a*). The two spectra were recorded under identical conditions, with excitation slits of 4.0 nm and emission slits of 2.5 nm, using an excitation wavelength of 340 nm. Although the ordinates in both spectra are in arbitrary units, they are scaled correctly relative to one another, as evidenced by the amplitude of the ~384 nm feature in each due to the MOPS buffer.

RESULTS

Amine-terminated SAMs were chosen to tether Ca^{2+}-ATPase to the surfaces of solid substrates based on the protein's putative structure derived from its primary amino acid sequence (MacLennan et al., 1985). Inspection of this putative structure in conjunction with the amino acid sequence revealed the existence of a concentration of negatively charged amino acid residues in the "headpiece" region of the enzyme. Because the transmembrane domain and the lumenal surface of the enzyme have comparatively few negatively charged residues, we reasoned that an amine-terminated SAM could be used not only to tether the protein to solid substrates, but also to form vectorially oriented monolayers of Ca^{2+}-ATPase.

Fig. 2 *a* shows a typical fluorescence emission spectrum from a single monolayer of 1,5-IAEDANS-labeled, detergent-solubilized Ca^{2+}-ATPase specifically bound to the surface of an amine-terminated SAM, after the sample had been suitably washed in low-ionic-strength buffer so as to remove nonspecifically bound protein. The emission maximum at ~476 nm is consistent with that reported in the literature (474 nm) (Squier et al., 1987). The narrow peak at ~384 nm is due to the MOPS buffer that was in the cuvette with the quartz substrate/amine SAM/Ca^{2+}-ATPase to maintain the hydration and pH of the sample. Because low ionic strength buffer can be used to remove nonspecifically bound protein without eliminating the fluorescence signal,

there appears to be a specific interaction between the amine-terminated SAM and the protein. The primarily electrostatic mode of binding was verified by washing such specimens in high-ionic-strength medium (0.1 M KCl in detergent buffer), which resulted in a decrease in the baseline fluorescence from the same sample previously washed in low-ionic-strength buffer, indicating a disruption of the electrostatic interaction between the amine-terminated SAM and the enzyme. (However, a total elimination of the fluorescence signal was not observed. See Discussion for further comments on this phenomenon.) Further evidence for electrostatic binding was provided by a control experiment, which showed that quartz substrates possessing methyl-terminated SAMs incubated in 1,5-IAEDANS-labeled, detergent-solubilized Ca^{2+}-ATPase for 22 h exhibited no fluorescence after washing in low-ionic-strength buffer. The specificity of the amine-terminated SAM for the "headpiece" of the enzyme was demonstrated by incubating quartz substrates possessing amine-terminated SAMs in unsolubilized, 1,5-IAEDANS-labeled pure SR, i.e., a dispersion of unilamellar SR vesicles whose surfaces expose only the enzyme's "headpiece." Fig. 2 *b* shows the fluorescence emission spectrum for such a sample, after washing with low-ionic-strength buffer. The emission maximum at ~476 nm is approximately two times that for the detergent-solubilized enzyme samples, as would be expected for a monolayer of unilamellar SR vesicles. The amine-terminated SAM/Ca^{2+}-ATPase monolayers on quartz substrates used for the fluorescence measurements were prepared *identically* and *simultaneously* with those on the Ge/Si multilayer substrates, so that protein binding measurements could be directly compared to the profile structures derived from the meridional x-ray diffraction data by x-ray interferometry and x-ray holography. The Ca^{2+}-ATPase was labeled with 1,5-IAEDANS for both types of specimens.

The meridional x-ray diffraction data for a typical bare Ge/Si multilayer substrate, for the same substrate with a "protected amine" SAM chemisorbed to its surface, and for the same substrate/amine-terminated SAM with detergent-solubilized Ca^{2+}-ATPase electrostatically bound, are shown in Fig. 3, *a*, *b*, and *c*, respectively, as $\log[I(q_z)]$. The absolute electron density profile, $\rho_{abs}(z)$, for these specimens can be expressed as

$$\rho_{abs}(z) = \bar{\rho}(z) + \Delta\rho(z), \tag{1}$$

where $\bar{\rho}(z)$ is the mean electron density profile and $\Delta\rho(z)$ is the electron density contrast profile, or the fluctuations about the mean electron density. The mean electron density profile gives rise to the specular x-ray scattering from the specimen's surface in the dynamical diffraction limit, especially for $q_z \leq (q_z)_{crit}$, whereas the electron density contrast profile gives rise to the kinematical meridional x-ray diffraction over all q_z (Blasie et al., 1992; Xu et al., 1993; Murphy et al., 1993). Because we were primarily concerned with the kinematical diffraction within these data, the ω-oscillations were therefore not extended down to the critical

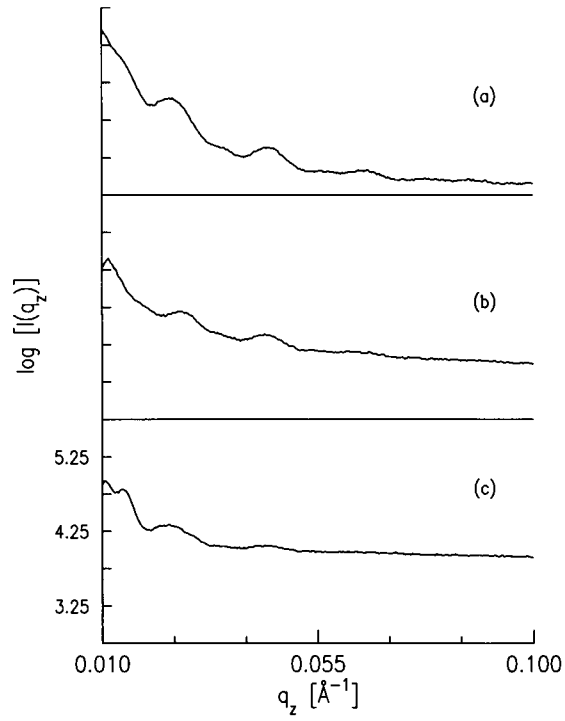

FIGURE 3 Meridional x-ray scattering data, $\log[I(q_z)]$, for (*a*) a bare, two-unit cell Ge/Si multilayer substrate, (*b*) a "protected amine" SAM covalently bound to the substrate in *a*, and (*c*) detergent-solubilized Ca^{2+}-ATPase electrostatically bound to the Ge/Si multilayer/11-siloxyundecaneamine SAM in *b*. The abscissa is the reciprocal space coordinate, q_z ($Å^{-1}$), and the ordinate is the logarithm of counts collected. The ordinate values for *a* and *b* are the same as those shown for *c*.

angle for specular scattering from the specimen's surface, but were instead stopped at the equivalent reciprocal space $(q_z)_{min} \approx 0.01$ $Å^{-1}$. For the specimens studied, meridional x-ray scattering above background levels with a signal-to-noise ratio in excess of 2:1 was generally observed out to $(q_z)_{max} \sim 0.09$ $Å^{-1}$.

The meridional x-ray scattering intensity data, $I(q_z)$, arising from the absolute electron density profile, can be expressed as:

$$I(q_z) = |F_{tot}(q_z)|^2 = |F_{spec}(q_z)|^2 + |F_{kin}(q_z)|^2 + 2F_{spec}(q_z)F_{kin}(q_z). \tag{2}$$

For $q_z > (q_z)_{crit}$, $|F_{spec}(q_z)|$ approaches zero rapidly and monotonically, and thus $|F_{tot}[q_z > (q_z)_{crit}]|^2 \rightarrow |F_{kin}(q_z)|^2$. Therefore, the total meridional x-ray scattering data from these specimens, $I(q_z)$ for $(q_z)_{crit} < (q_z)_{min} \leq q_z \leq (q_z)_{max}$, are dominated by the kinematical diffraction arising from the electron density contrast profile, $\Delta\rho(z)$.

For the inorganic multilayer substrate plus SAM/enzyme overlayer system described here, the Ge/Si multilayer substrate has very narrow, large-amplitude features in its electron density contrast profile, and its profile structure is essentially known from its fabrication specifications. The

SAM/enzyme overlayers make a relatively small contribution to the profile structure of the composite system, because their electron density contrast profiles are expected to contain broad, low-amplitude features as compared to those in the profile of the Ge/Si multilayer substrate. Thus we can use the known profile structure of the Ge/Si multilayer substrate to determine the profile structure of the SAM/enzyme overlayers by x-ray interferometry (Lesslauer and Blasie, 1971), as described below. The kinematical meridional x-ray diffraction for the composite structure, as shown in Fig. 3 *c*, is given by

$$|F_{kin}(q_z)|^2 = |F_k(q_z)|^2 + |F_u(q_z)|^2 + 2|F_k(q_z)||F_u(q_z)|\cos\{[\Psi_k(q_z) - \Psi_u(q_z)] + [2\pi q_z A_{ku}]\}, \quad (3)$$

where $|F_{kin}(q_z)|^2$ is the total kinematical structure factor modulus squared of the composite structure and $|F_k(q_z)|^2$ and $|F_u(q_z)|^2$ are the kinematical structure factor moduli squared of the known multilayer substrate and the unknown SAM/enzyme overlayers, respectively. These three structure factor moduli are obtainable from the kinematical x-ray diffraction from the composite system, from the Ge/Si multilayer substrate itself, and from the SAM/enzyme overlayers on a uniform Si substrate. Ψ_k and Ψ_u are the phases of their respective structure factors, each referenced to the center of mass of its respective profile structure. Ψ_k is known, because the reference profile structure of the Ge/Si multilayer substrate (and, therefore, its structure factor) is known and Ψ_u is unknown. A_{ku} is the distance along the z axis between the center of mass of the Ge/Si multilayer substrate and the SAM/enzyme overlayers. If the mathematical substitution $\Psi'_u = [\Psi_u - A_{ku}]$ is made, we then reference the center of mass of the profile of the unknown overlayer structure to the center of mass of the profile of the known multilayer reference structure (Chupa et al., 1994). Solving for the only remaining unknown Ψ'_u allows determination of the unknown profile structure of the SAM/enzyme overlayer. The third term in Eq. 3 represents the critical interference between the Ge/Si multilayer substrate and the SAM or the SAM/enzyme overlayer structures. Its effect can be seen by examining the differences between the meridional x-ray diffraction data of the Ge/Si multilayer substrate itself and that of the substrate plus "protected amine" SAM and the composite multilayer substrate/amine SAM/enzyme systems shown in Fig. 3, *a*, *b*, and *c*, respectively.

For $q_z \geq 0.0093$ Å^{-1}, $|F_{kin}(q_z)|^2$ for the bare Ge/Si multilayer substrate, the substrate plus "protected amine" SAM, and the composite multilayer substrate/amine SAM/enzyme systems was obtained from their Lorentz-corrected, meridional elastic x-ray scattering, $I_c(q_z)$, by subtraction of $|F_{spec}(q_z)|^2$, as approximated by the Lorentz-corrected meridional scattering from a uniform silicon substrate (Xu et al., 1993; Murphy et al., 1993). A Lorentz factor q_z was applied to correct for the ω-oscillations of the specimens (Skita et al, 1986). This procedure resulted in the kinematical diffraction data being restricted to the q_z range $(q_z)_{min} \approx 0.0103$ Å$^{-1} \leq q_z \leq (q_z)_{max} \approx 0.092$ Å^{-1}. All Fourier analyses, via both interferometry and holography, were restricted to this q_z window. A $(q_z)_{max}$ of ~0.09 Å^{-1} is consistent with the full width at half-maximum of the broadest Ge peak in the substrate.

The evidence of destructive interference phenomena upon addition of the overlayer structures to the Ge/Si multilayer substrate is not so readily apparent in Fig. 3, as has been demonstrated previously for other similarly tethered proteins such as photosynthetic reaction centers (Chupa et al., 1994) and cytochrome *c* oxidase (Edwards et al., manuscript in preparation). It then becomes useful to view these data instead as their corrected meridional intensity functions, expressed as a function of the reciprocal space coordinate, q_z (Å^{-1}), shown in Fig. 4. The overall lengthening of the profile structure of the system in the z-direction upon formation of the "protected amine" SAM and, subsequently, the amine-terminated SAM/enzyme overlayers manifests itself most clearly by changes in the kinematical meridional

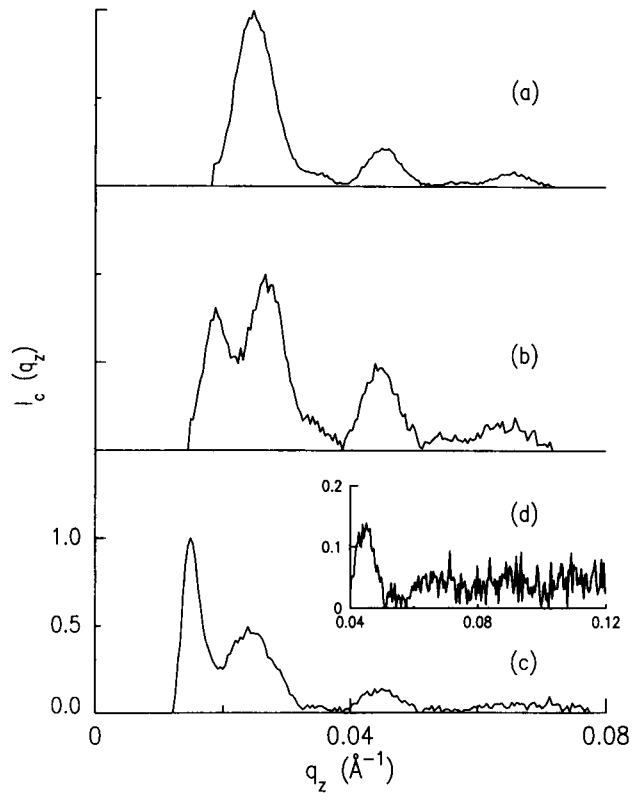

FIGURE 4 The corrected (see Results) meridional intensity functions $I_c(q_z)$ for the data shown in Fig. 3 for (*a*) the bare, two-unit cell Ge/Si multilayer substrate, (*b*) the "protected amine" SAM covalently bound to the substrate in *a*, and (*c*) detergent-solubilized Ca^{2+}-ATPase electrostatically bound to the Ge/Si multilayer substrate/11-siloxyundecaneamine SAM in *b*. Displayed in *d* are the data in *c* on an expanded ordinate scale, starting at 0.04 Å^{-1} and extending to 0.12 Å^{-1}. The low-frequency fluctuations, namely the three broad maxima, over this range of q_z are the kinematical diffraction data.

x-ray diffraction primarily at low q_z. This constructive interference phenomenon is demonstrated in Fig. 4, *b* and *c*, for $q_z < 0.030$ Å^{-1}. Also evident in these intensity functions are systematic changes in peak amplitudes and their ratios upon addition of the overlayer structures. Fig. 4 *d* displays the data in Fig. 4 *c* on an expanded ordinate scale, starting at $q_z = 0.04$ Å^{-1} and extending to $q_z = 0.12$ Å^{-1}. In spite of the counting statistics dominated by high-frequency noise over this range of q_z, the low-frequency fluctuations due to the kinematical diffraction in this data are readily discernible, even without unbiased smoothing. Thus, the maximum fluctuation within 0.05 Å$^{-1} \leq q_z \leq 0.08$ Å^{-1}, with a signal-to-noise ratio of ~3:1, has been included in our analysis, resulting in a minimum wavelength component or resolution of ~12 Å in our derived profiles, whereas the kinematical diffraction data extend to an equivalent resolution of ~8 Å.

X-ray interferometric analysis of the meridional kinematical x-ray diffraction data was performed, utilizing a highly constrained real-space refinement algorithm as described previously (Xu et al., 1991) to accomplish the interferometric phasing of these data. The procedure involved first establishing the relative electron density profile for the bare Ge/Si multilayer substrate, with the initial models for the substrate being constructed on an absolute electron density scale based on the fabrication specifications. These models were then initially relaxed via a model refinement analysis, by comparing the calculated structure factor modulus squared and its unique Fourier transform, the Patterson function, for the models with their corresponding experimental meridional diffraction data and Patterson functions, subject to the same q_z window as the experimental meridional x-ray diffraction data [$(q_z)_{min} \approx 0.0103$ Å$^{-1} \leq q_z \leq (q_z)_{max} \approx 0.092$ Å^{-1}]. Once "reasonable" (i.e., close but not perfect) agreement had been achieved between the experimental functions and their model counterparts, estimated by a least-squares analysis, the constrained real-space refinement algorithm was employed as a final relaxation procedure. The interior portion of the so-refined model relative electron density profile for the bare Ge/Si multilayer substrate, $[\Delta\rho_{mod}(z)]_{substrate}$ (i.e., $Ge_2Si_{30}Ge_2$), was utilized as the primary constraint. This procedure yielded the experimental relative electron density profile for the bare substrate, $[\Delta\rho_{exp}(z)]_{substrate}$, which exactly predicted both the experimental intensity and Patterson functions. Only the interior portion of this "known" relative electron density profile structure was then used as the reference structure for the constrained real-space refinement of the meridional x-ray diffraction for the multilayer substrate/amine SAM/enzyme system because of the modification of the outer silicon layer of the substrate that occurs upon formation of the SAM on its surface by chemisorption (Xu et al., 1993).

The highly constrained real-space refinement algorithm yields one solution to a finite number of possible solutions for the phase of the kinematical structure factor, using the phase dominance of the known reference structure to force the box-refinement algorithm to converge to the local structure most similar to the reference structure (Stroud and Agard, 1979; Makowski, 1981). X-ray holography (Lesslauer and Blasie, 1971; Smith, 1969) was used to prove the correctness of the experimental relative electron density profiles for the composite systems derived via x-ray interferometry. If the Ge layers within the reference profile structure of the Ge/Si multilayer substrates are sufficiently narrow (as is possible with MBE fabrication) and A_{ku} is sufficiently large, then the unknown profile structure for the SAM/enzyme overlayer is reconstructed with minimal distortion at the edge of the Patterson function, $P(z)$, which is uniquely obtained by Fourier transformation of the kinematical meridional x-ray diffraction data without any phase information.

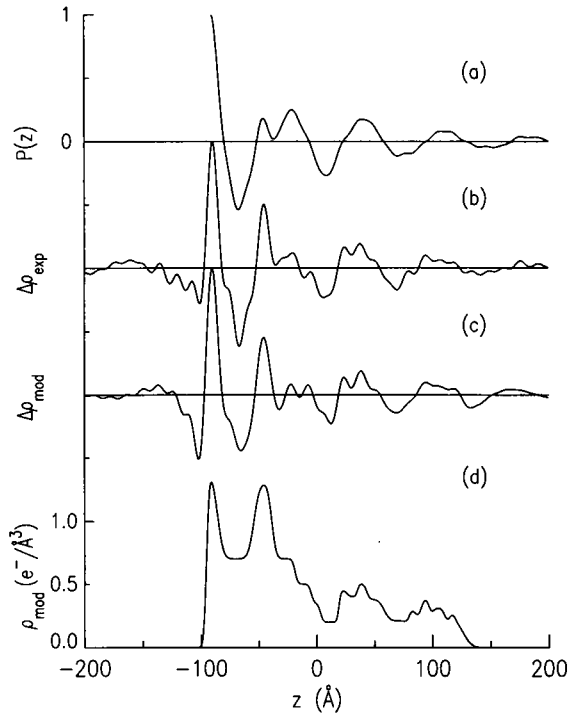

FIGURE 5 Illustration of the various functions employed in the determination of the profile structure of Ca^{2+}-ATPase tethered to a $2(Ge_2Si_{30})$ multilayer substrate via an amine-terminated SAM. (*a*) The experimental Patterson function, $P(z)$, uniquely derived from the x-ray diffraction data without any phase information. (*b*) The experimental relative electron density profile, $\Delta\rho_{exp}(z)$. (*c*) The refined model relative electron density profile, $\Delta\rho_{mod}(z)$, calculated via a unique Fourier transform-inverse Fourier transform of *d*. (*d*) The refined model absolute electron density, $\rho_{mod}(z)$, in units of e^-/Å^3. See text and references (Blasie et al., 1992; Chupa et al., 1994; Murphy et al., 1993; Xu et al., 1993) for further details.

The various aspects of the determination of the profile structure of Ca^{2+}-ATPase tethered to a multilayer substrate are illustrated in Fig. 5. Fig. 5 *b* shows the experimental relative electron density profile structure, $\Delta\rho_{exp}(z)$, for the composite Ge/Si multilayer substrate/amine SAM/Ca^{2+}-ATPase system, derived by applying the constrained real-space refinement to the specimen's meridional x-ray diffraction data, using the reference structure as the primary

constraint. The two prominent peaks of density correspond to the Ge_2 layers in the multilayer substrate. After the formation of the amine SAM and the Ca^{2+}-ATPase layers on the surface of the substrate, additional, more complex features appear beyond the SiO_x surface of the substrate for $0\ Å \leq z \leq 130\ Å$. To understand the nature and source of these new features, a real-space model on an absolute electron density scale was constructed to account for each feature. Fig. 5 *d* shows the refined model absolute electron density profile $\rho_{mod}(z)$ for the Ge/Si multilayer substrate/amine SAM/Ca^{2+}-ATPase system, which accounts for each feature in $\Delta\rho_{exp}(z)$ (Fig. 5 *b*), as demonstrated by a comparison of Fig. 5 *b* with Fig. 5 *c*, the model relative electron density profile, $\Delta\rho_{mod}(z)$. $\Delta\rho_{mod}(z)$ is uniquely calculated by a "double" Fourier transform (i.e., Fourier transform–inverse Fourier transform) of $\rho_{mod}(z)$ subject to the experimental q_z window. Finally, comparison of Fig. 5 *b* with the Patterson function $P(z \geq 0)$ shown in Fig. 5 *a* for $0\ Å < z < 150\ Å$ (the origin of which has been offset horizontally to correspond with the first Ge_2 peak in $\Delta\rho_{exp}(z)$ for ease of comparison) demonstrates that the amine SAM/Ca^{2+}-ATPase overlayer features in the derived electron density contrast profile, $\Delta\rho_{exp}(z)$, are indeed reconstructed at the edge of the Patterson function, thereby proving $\Delta\rho_{exp}(z)$ correct over the region of interest via x-ray holography. A one-to-one correspondence between each feature in the refined model relative electron density profile and its counterpart in the experimental relative electron density profile established both the position (± 0.1 Å) and electron density level ($\pm 0.01\ e^-/Å^3$) of each feature in the so-refined $\rho_{mod}(z)$ (see Murphy et al., 1993, for the basis for these precisions). In Fig. 5 *d*, the substrate profile occurs within $-100\ Å < z < 0$ Å, with the two peaks at $z \approx -92$ Å and $z \approx -47$ Å in Fig. 5 *c* arising from the two Ge_2 layers in the substrate. (The two interfaces representing Si/SiO_x and SiO_x/SiO_x occur at $z \approx -19$ Å and $z \approx -6.5$ Å in Fig. 5 *d*, and give rise to the small peaks at $z \approx -23.5$ Å and $z \approx -8$ Å in Fig. 5 *c*. These variable-density SiO_x layers are formed during the cleaning procedures before chemisorption of the amine SAM to the surface of the substrate, as mentioned above (Xu et al., 1993). Precise agreement between $\Delta\rho_{mod}(z)$ (Fig. 5 *c*) and $\Delta\rho_{exp}(z)$ (Fig. 5 *b*) in the region $-19\ Å < z < 0$ Å depends on the precise positioning of the SiO_x features to within 0.1 Å. Although this specimen was not modeled to the point of achieving exact agreement in this region (see Discussion for the resolution of this disparity), a reasonably good model has nevertheless been achieved.) The amine SAM profile occurs within $0\ Å < z < 20$ Å in Fig. 5 *d*, and the SiO_x/SAM interface accounts for the inflection at $z \approx 8$ Å in Fig. 5 *c*. The Ca^{2+}-ATPase profile occurs within $20\ Å < z < 130$ Å in Fig. 5 *d*. The enzyme's profile contains only broad, relatively low-amplitude features and extends over a profile width of ~110 Å (FWHM), which is consistent with a monolayer of fully hydrated Ca^{2+}-ATPase (see Discussion).

DISCUSSION

We have demonstrated the ability to form vectorially oriented monolayers of detergent-solubilized Ca^{2+}-ATPase from the sarcoplasmic reticulum by tethering the enzyme to solid substrates via self-assembled monolayers (SAMs) possessing surface endgroup specificity for the enzyme. Fluorescent labeling of the enzyme in conjunction with the formation of these monolayers on quartz substrates allowed the determination of the nature of protein binding via fluorescence spectroscopy. First, the protein binding was thereby demonstrated to be highly reproducible. Second, comparison of the fluorescence emission spectra for the detergent-solubilized Ca^{2+}-ATPase with those for unilamellar vesicles of isolated SR bound to the amine-terminated SAMs on quartz demonstrated specific binding of Ca^{2+}-ATPase via the "headpiece." Third, the reversibility of the protein binding was demonstrated by employing high-ionic-strength buffer to dissociate the specifically bound protein from the amine-terminated SAMs, as evidenced by the reduction in the fluorescence intensity from such a sample, as opposed to the same sample rinsed further with low-ionic-strength buffer only. The inability to totally eliminate the fluorescence signal might suggest that the interaction between Ca^{2+}-ATPase and the amine-terminated SAM is not solely electrostatic (polar) in nature, but instead may be some combination of polar and nonpolar interactions. It is possible that there is some minor local unfolding of the tertiary structure of Ca^{2+}-ATPase that enables it to penetrate into the amine-terminated SAM and allows interaction between its hydrophobic residues and the hydrocarbon chains of the SAM. Such a phenomenon has been similarly observed for cytochrome *c* electrostatically bound to a charged lipid headgroup, where the protein binding was also found to be only partially reversible (Pachence and Blasie, 1991). This phenomenon has also been demonstrated theoretically in molecular dynamics simulations of yeast cytochrome *c* bound to a thiol-terminated SAM in the absence of water, where local unfolding of the protein was observed to occur at the SAM/protein interface (Tobias et al., unpublished results). However, the observed partial reversibility of enzyme binding in our case might also be due to the "inaccessibility" of the high-ionic-strength medium to the amine-terminated SAM/Ca^{2+}-ATPase interface. This may result from a "fusion" of the annular rings of detergent molecules that solvate the enzyme molecules in the monolayer, thereby impeding penetration of the high-ionic-strength medium to the amine SAM/enzyme region of the specimen and prohibiting a disruption of the electrostatic interaction between them.

Finally, the relative fluorescence intensity observed for the detergent-solubilized Ca^{2+}-ATPase bound to amine-terminated SAMs on quartz suggests a maximum in-plane density of ~90% of close packing. This estimation was made through the use of a calibration curve based on solutions of detergent-solubilized, 1,5-IAEDANS-labeled Ca^{2+}-ATPase of known concentration. However, this estimate of

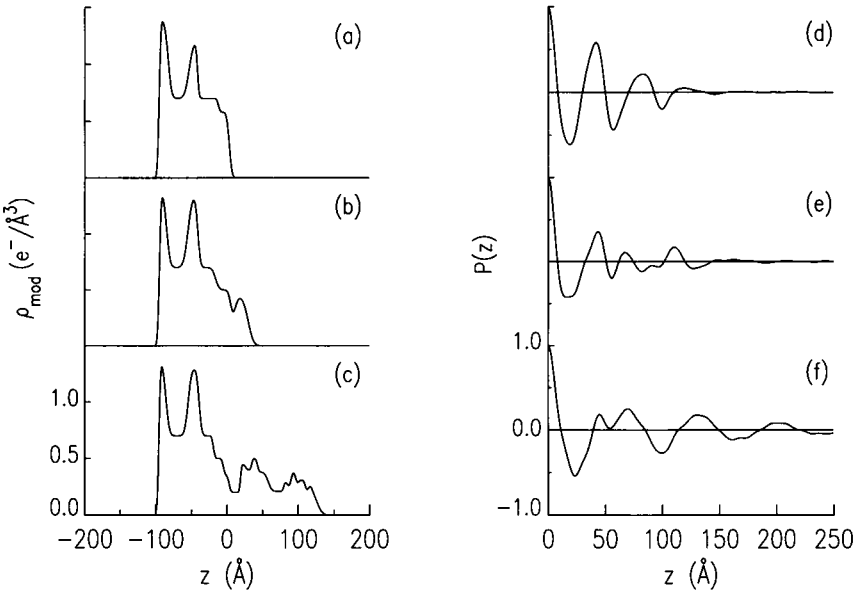

FIGURE 6 (*a–c*) The refined model absolute electron density profiles, $\rho_{mod}(z)$, for (*a*) a bare, two-unit cell Ge/Si multilayer substrate, (*b*) a "protected amine" SAM covalently bound to the substrate in *a*, and (*c*) detergent-solubilized Ca^{2+}-ATPase electrostatically tethered to the multilayer substrate/amine-terminated SAM in *b*, derived from x-ray interferometric analysis of the corrected meridional x-ray diffraction data shown in Fig. 4. (*d–f*) The experimental Patterson functions, $P(z \geq 0)$, for the specimens described in *a*, *b*, and *c*, respectively, calculated uniquely from the data shown in Fig. 4 without any phase information.

the in-plane density of the enzyme may be high by a factor of 2–3, because of two factors. The first is due to possible polarization effects arising from the fluorimeter optics, grazing incidence, and the vectorial orientation of the enzyme. In addition, the grazing incidence geometry itself may cause an enhanced fluorescence emission signal to be observed. Such an estimate is in agreement with preliminary atomic force microscopy (AFM) experiments on these Ca^{2+}-ATPase monolayers. The AFM images indicate large 600-1000-Å-diameter domains of the enzyme in single monolayer thickness (~100 Å) randomly distributed over the SAM surface with greater than 50% but less than 100% coverage.

Formation of Ca^{2+}-ATPase monolayers on inorganic multilayer substrates formed by molecular beam epitaxy allowed the determination of the profile structure for the system by x-ray interferometry and proof of the correctness of these so-derived profile structures by x-ray holography, to a spatial resolution of ~12 Å. This resolution was sufficient to establish the vectorial orientation of the enzyme within these monolayers. Fig. 6 shows the refined model absolute electron density profiles, $\rho_{mod}(z)$, for a bare substrate (Fig. 6 *a*), the bare substrate in Fig. 6 *a* possessing a covalently bound "protected amine" SAM (Fig. 6 *b*), and detergent-solubilized Ca^{2+}-ATPase electrostatically tethered to the Ge/Si multilayer substrate/amine-terminated SAM in Fig. 6 *b* (Fig. 6 *c*), derived by x-ray interferometric analysis of the meridional x-ray diffraction data shown in Fig. 4 for each case. Clearly visible in Fig. 6 *b* is the additional feature that appears beyond the surface of the bare substrate in Fig. 6 *a* upon chemisorption of the "protected amine" SAM on its surface. The peak in Fig. 6 *b* at $z \approx 20$ Å is attributed to the protecting *tert*-butoxycarbonyl group of the SAM. The "protected amine" SAM has a profile width of ~17 Å, which is consistent with its structure. Upon activation of the "protected amine" SAM (see Materials and Methods) this peak disappears, and upon formation of the electrostatically bound monolayer of Ca^{2+}-ATPase it is replaced in Fig. 6 *c* by the broad feature from 20 Å $< z <$ 130 Å, which is indicative of a single monolayer of Ca^{2+}-ATPase, with its long axis aligned perpendicular to the plane of the substrate. Shown in Fig. 6 *d–f* are the experimental Patterson functions, $P(z)$, for $z \geq 0$ for the specimens described in Fig. 6, *a*, *b*, and *c*, derived from the meridional x-ray diffraction data shown in Fig. 4 without any phase information. In addition to their utilization in the holographic aspect of our data analysis, the Patterson functions further demonstrate the increase in thickness of the structure of the system upon formation of the SAM and SAM/enzyme overlayers.

Fig. 7 shows the refined model absolute electron density profiles for two different Ge/Si multilayer substrates with amine-terminated SAMs and tethered detergent-solubilized Ca^{2+}-ATPase. The profiles in Fig. 7, *a* and *b*, possess the same features throughout; the Ge/Si multilayer substrate, SiO_x layers, amine-terminated SAM, and Ca^{2+}-ATPase features are all readily discernible and occur at approximately the same *z* position in each profile. It is interesting to note, however, that the two samples possess different in-plane densities of the amine-terminated SAM, as can be seen by inspection of the 0 Å $< z <$ 20 Å region in the two profiles. The SAM in Fig. 7 *b* possesses a relatively lower in-plane density as compared to the SAM of Fig. 7 *a*, as its absolute electron density is lower and its profile length is shorter (0.2 e^-/Å^3 and 15.7 Å for Fig. 7 *a* vs. 0.13 e^-/Å^3 and 10.5 Å for Fig. 7 *b*). As a result, the in-plane density of the tethered detergent-solubilized Ca^{2+}-ATPase is also lower, as indicated by the uniformly lower electron density throughout the profile structure of the enzyme for 20 Å $< z <$ 130 Å, yet there is not a significant change in its profile structure.

The profile widths of the Ca^{2+}-ATPase features within the profile structures for these specimens shown in Fig. 7

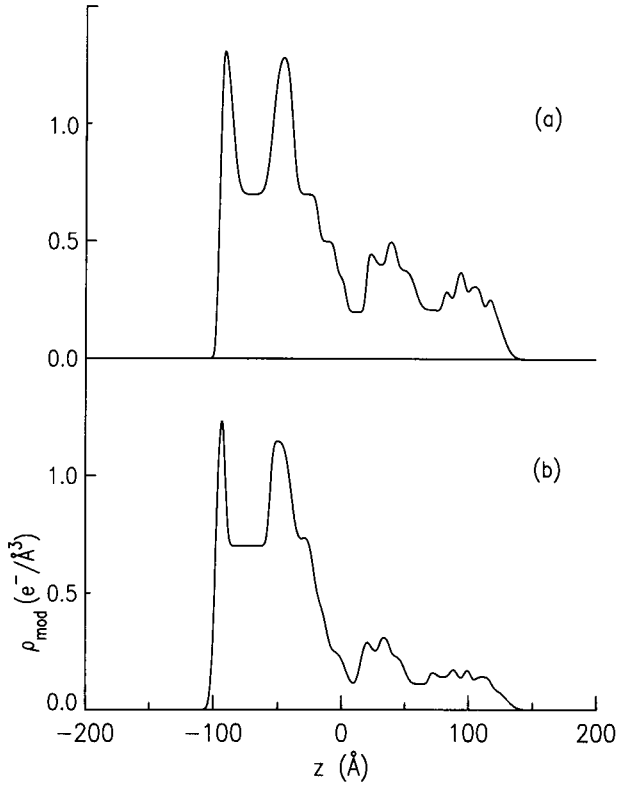

FIGURE 7 Absolute electron density profiles, $\rho_{mod}(z)$, for two separate Ge/Si multilayer substrate/amine-terminated SAM/Ca^{2+}-ATPase specimens, derived via x-ray interferometry and proved correct via x-ray holography, for two different in-plane densities of the amine-terminated SAM. *a* Shows a higher density SAM in the 0 Å $< z <$ 20 Å region of the profile as compared to the same region in *b*, which shows a SAM of lower absolute electron density and shorter profile length. As a result, the in-plane density of the electrostatically tethered Ca^{2+}-ATPase in *b* is also uniformly lower, but without any significant change in its profile structure.

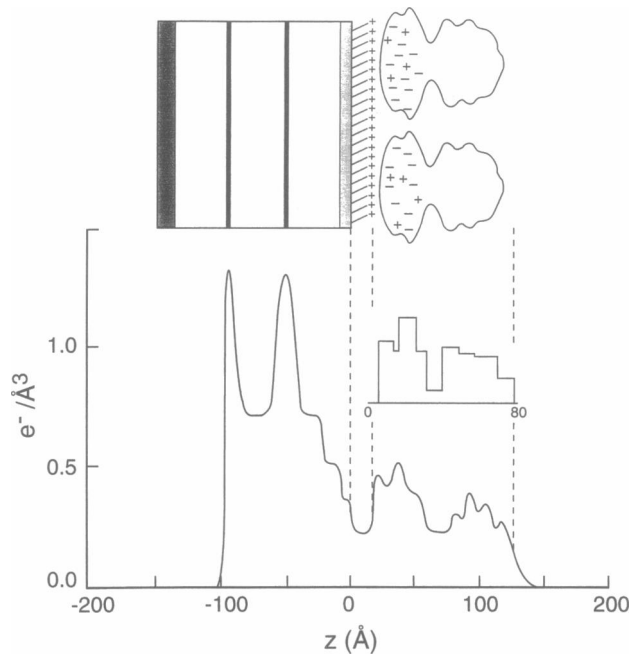

FIGURE 8 A comparison between the refined absolute electron density model, $\rho_{mod}(z)$, in units of e^-/Å^3, derived via x-ray interferometry/holography in the present study on detergent-solubilized Ca^{2+}-ATPase monolayers with the step-function model profile, in units of Å^2, derived from the combined x-ray and neutron diffraction experiments performed previously on partially dehydrated, oriented SR membrane multilayers (Herbette et al., 1985). Note that the abscissa scale for the step-function model profile is 80 Å in length. The schematic representation of the system is provided for comparison, shown approximately to scale. The vertical lines indicate the correlation between the structures in the schematic and the features in the absolute electron density profile. Clearly discernible are the "headpiece," "stalk," and "transmembrane" domains of the enzyme in the two models, with the "headpiece" of the enzyme shown in the step-function model profile being compressed in the oriented multilayer case relative to that for the tethered monolayer. Comparison of these two results is possible even though they are viewed with different ordinate units, because the figure in the inset was derived assuming that the protein possesses uniform internal mass density along the *z* axis.

confirm single monolayer coverage by Ca^{2+}-ATPase. The tethered Ca^{2+}-ATPase was found to have an average profile width of ~110 Å, which corresponds to a single monolayer in which the long axis of the protein is oriented perpendicular to the monolayer plane. This profile width is consistent with that for the enzyme within the isolated SR membrane (Herbette et al., 1985). A comparison between the results of the current study and those of Herbette et al. (1985) is shown in Fig. 8, which shows the refined model absolute electron density profile, $\rho_{mod}(z)$, for the specimen shown in Figs. 5 *d*, 6 *c*, and 7 *a* and the step-function model profile derived from the combined x-ray and neutron diffraction experiments of the previous study directly above. In this previous study, x-ray and neutron diffraction were used to determine the separate profile structures of the water, lipid, and protein components of the isolated SR membrane, as both oriented SR multilayers and vesicular dispersions, at ~11 Å resolution. The SR preparation utilized in these experiments was the "pure" form, in which ~90% of the total protein present is Ca^{2+}-ATPase. These experiments demonstrated that ~50% of the mass of the total protein lies outside the lipid bilayer in the cytoplasm, in what we call the "headpiece" of the enzyme. For both the oriented multilayers and the vesicular dispersions the "transmembrane" domain of the enzyme, or the portion of the Ca^{2+}-ATPase that spans the lipid bilayer, was found to have a profile width of ~40 Å. In contrast, the "headpiece" portion of the enzyme was found to have a variable profile width depending upon the environment. The total profile width of the Ca^{2+}-ATPase was determined to be 75–77 Å in maximally "compressed" (partially dehydrated) oriented SR multilayers and 86–88 Å in more hydrated oriented SR multilayers, whereas a total profile width of ~100 Å was found for Ca^{2+}-ATPase in fully hydrated SR vesicular dispersions. This latter result for the unilamellar vesicular dispersions agrees well with the present study, indicating that we are observing the detergent-solubilized Ca^{2+}-ATPase in these vectorially oriented monolayers with its "headpiece" in an

uncompressed, fully hydrated state. The schematic representation of the Ge/Si multilayer substrate/amine SAM/Ca^{2+}-ATPase system has been provided in Fig. 8, shown approximately to scale. The vertical lines demonstrate the positions of the different features within the profile, namely the substrate, SAM, and enzyme. Recalling that the enzyme possesses an asymmetric structure in the z-direction (Herbette et al., 1985), we can correlate the "headpiece" region of the enzyme in the schematic with the region ~ 20 Å $< z < 66$ Å in the refined model absolute electron density profile, the "stalk" portion of the enzyme with ~ 66 Å $< z < 79$ Å, and the "transmembrane" domain of the enzyme with the region ~ 79 Å $< z < 130$ Å. The strong inherent asymmetry in the enzyme portion of the profile structure verifies the formation of a vectorially oriented monolayer of Ca^{2+}-ATPase (see Chupa et al., 1994). Examination of Fig. 8 shows that the "headpiece" region shown in the step-function model profile is more compressed for the partially dehydrated, oriented multilayer of isolated membranes than it is for the fully hydrated, tethered monolayer in the refined model absolute electron density profile of the present study. It should be pointed out that the two separate profiles can be compared, even though they possess different ordinate units (electron density for the tethered monolayer and area for the oriented multilayer), because the area profile that resulted from the x-ray and neutron diffraction data analysis includes the assumption that the protein had uniform internal mass density as a function of z.

The effects of the $(q_z)_{min}$ truncation can be eliminated from the experimental relative electron density profiles, $\Delta\rho_{exp}(z)$, by adding the (very low resolution) mean electron density profile, $\bar{\rho}_{mod}$, for the refined model absolute electron density profile, to produce a profile that contains only $(q_z)_{max}$ truncation (see Eq. 1). Fig. 9 *a* shows the resulting experimental absolute electron density profile for the Ge/Si multilayer substrate/amine SAM/Ca^{2+}-ATPase specimen described in Fig. 5. The corresponding refined model absolute electron density profile is shown in Fig. 9 *b*, which was modeled until its "double" Fourier transform, $\Delta\rho_{mod}(z)$, agreed with $\Delta\rho_{exp}(z)$ virtually precisely. Therefore, any differences between ρ_{abs} and ρ_{mod} in Fig. 9 over the regions more precisely modeled arise from the effects of $(q_z)_{max}$ truncation only. For example, for -100 Å $\leq z \leq -25$ Å within the unperturbed substrate region of these profiles, the differences arise from the simple effect of having only three wavelengths occurring between the two Ge peaks. Fig. 9 *a* also demonstrates that it was in fact unnecessary to try to model the SiO_x region of the specimen precisely, because addition of $\bar{\rho}_{mod}$ to $\Delta\rho_{exp}(z)$ shows us exactly what this region looks like.

Now that it has been demonstrated that vectorially oriented monolayers of detergent-solubilized Ca^{2+}-ATPase can be formed on the surfaces of solid substrates, we can begin to devise experiments that would probe the relationship between the structure of this enzyme and its function. For example, the inherent thinness of the protein monolayer permits low-energy resonance x-ray diffraction experiments

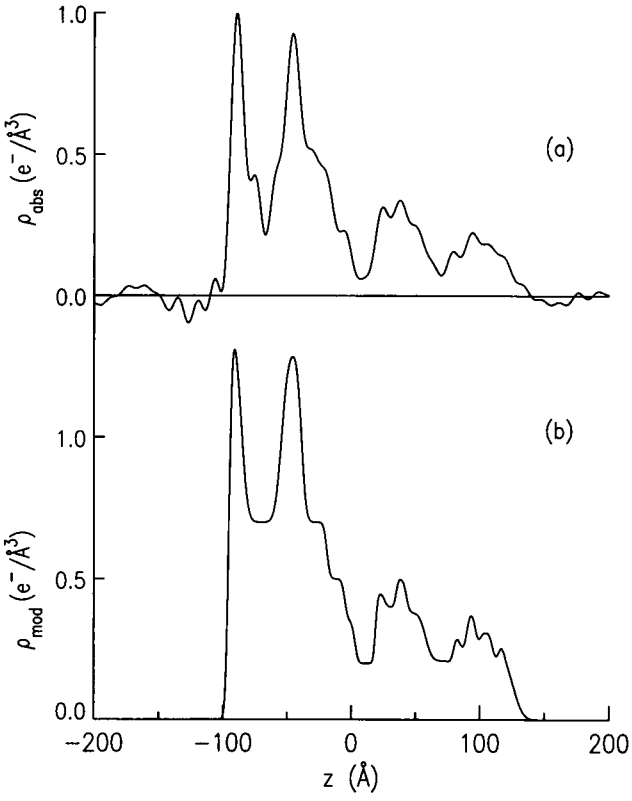

FIGURE 9 (*a*) Experimental absolute electron density profile, produced by summation of the mean electron density profile, $\bar{\rho}_{mod}(z)$, with the experimental relative electron density profile, $\Delta\rho_{exp}(z)$, to contain only $(q_z)_{max}$ truncation effects. (*b*) The refined model absolute electron density profile, $\rho_{mod}(z)$, for the Ge/Si multilayer substrate/amine-terminated SAM/Ca^{2+}-ATPase specimen, derived by x-ray interferometry and proved correct by x-ray holography.

about the Ca^{2+} K absorption edge that are not possible in thick multilayers of SR because of the strong absorption effects at such low x-ray energies. Such experiments would serve to locate the positions and occupancies of the Ca^{2+} binding sites directly within the profile structure of the enzyme and their evolution upon enzyme phosphorylation. Vectorially oriented monolayers of detergent-solubilized Ca^{2+}-ATPase tethered to Ge/Si multilayer substrates may provide a means of performing neutron diffraction experiments employing selective deuteration of the detergent $C_{12}E_9$ or the water used in the sample preparation to locate the detergent and water molecules within the profile structure of a single monolayer of the enzyme. (We expect that this detergent does not contribute to the above-described profile structures of single monolayers of the $C_{12}E_9$-solubilized Ca^{2+}-ATPase, because comparison between these profile structures and those for the enzyme within the isolated membrane show striking similarities. This detergent has an essentially uniform electron density over the length of the molecule, and such molecules should align with their long axes approximately parallel to the z axis, and therefore its presence most likely would not be noticed in these

profile structures.) Finally, vectorially oriented single monolayers of detergent-solubilized Ca^{2+}-ATPase may be useful in providing two-dimensional crystalline enzyme monolayers of long-range order that are necessary to obtain high-resolution, three-dimensional structures via electron microscopic 3-D image reconstruction techniques.

To be able to perform the correlative structure/function studies on such systems described here, we need to be able to measure the kinetics of Ca^{2+} transport directly in the monolayer. At the moment we assume that the protein is functional in the monolayer based on three considerations; namely, the Ca^{2+}-ATPase was functional before adsorption to the amine-terminated SAM, the monolayers are maintained at high relative humidity during the x-ray diffraction data collection, and the binding of the enzyme to the amine-terminated SAM can be shown to be at least partially reversible. Although it is difficult, we have at hand the technological capability for measuring ATP-induced Ca^{2+} occlusion and transport kinetics directly in the monolayers. Once such measurements have been made we will be in a position to examine at least the profile structure of the enzyme, including the distribution of calcium ions within this structure, in depth for each step in the reaction sequence that brings about Ca^{2+} transport by this enzyme, and, along with the emerging information concerning its three-dimensional structure, the goal of understanding active ion transport by the Ca^{2+}-ATPase of SR may be realized.

We would like to thank Dr. Michael J. Therien, Department of Chemistry, University of Pennsylvania, for graciously allowing the use of his Perkin-Elmer model LS50 luminescence spectrometer for the fluorescence measurements.

This work was supported by National Institutes of Health grant HL18708.

REFERENCES

Amador, S. M., J. M. Pachence, R. Fischetti, J. P. McCauley, Jr., A. B. Smith, III, and J. K. Blasie. 1993. Use of self-assembled monolayers to covalently tether protein monolayers to the surface of solid substrates. *Langmuir.* 9:812–817.

Asturias, F. J., and J. K. Blasie. 1991. Location of high-affinity metal binding sites in the profile structure of the Ca^{2+}-ATPase in the sarcoplasmic reticulum by resonance x-ray diffraction. *Biophys. J.* 59: 488–502.

Asturias, F. J., R. F. Fischetti, and J. K. Blasie. 1994a. Changes in the profile structure of the sarcoplasmic reticulum membrane induced by phosphorylation of the Ca^{2+}-ATPase enzyme in the presence of terbium: a time-resolved x-ray diffraction study. *Biophys. J.* 66:1653–1664.

Asturias, F. J., R. F. Fischetti, and J. K. Blasie. 1994b. Changes in the relative occupancy of metal-binding sites in the profile structure of the sarcoplasmic reticulum membrane induced by phosphorylation of the Ca^{2+}-ATPase in the presence of terbium: a time-resolved, resonance x-ray diffraction study. *Biophys. J.* 66:1665–1677.

Bean, J. C., L. C. Feldman, A. T. Fiory, S. Nakahara, and I. K. Robinson. 1984. Ge_xSi_{1-x}/Si strained-layer superlattice grown by molecular beam epitaxy. *J. Vac. Sci. Technol.* A2:436–440.

Bean, J. C., and E. A. Sadowski. 1982. Silicon MBE apparatus for uniform high-rate deposition on standard format wafers. *J. Vac. Sci. Technol.* 20:137–142.

Bigelow, D. J., T. C. Squier, and G. Inesi. 1992. Phosphorylation-dependent changes in the spatial relationship between Ca-ATPase polypeptide chains in sarcoplasmic reticulum membranes. *J. Biol. Chem.* 267:6952–6962.

Blasie, J. K., D. Pascolini, F. Asturias, L. G. Herbette, D. Pierce, and A. Scarpa. 1990. Large-scale structural changes in the sarcoplasmic reticulum membrane ATPase appear essential for calcium transport. *Biophys. J.* 58:687–693.

Blasie, J. K., S. Xu, M. Murphy, J. Chupa, J. P. McCauley, Jr., A. B. Smith, III, L. J. Peticolas, and J. C. Bean. 1992. Profile structures of macromolecular monolayers on solid substrates by X-ray interferometry/holography. *Mater. Res. Soc. Symp. Proc.* 237:399–409.

Chupa, J. A., J. P. McCauley, Jr., R. M. Strongin, A. B. Smith, III, J. K. Blasie, L. J. Peticolas, and J. C. Bean. 1994. Vectorially oriented membrane protein monolayers: profile structures via x-ray interferometry/holography. *Biophys. J.* 67:336–348.

Coll, R. J., and A. J. Murphy. 1984. Purification of the CaATPase of sarcoplasmic reticulum by affinity chromatography. *J. Biol. Chem.* 259: 14249–14254.

Cowley, J. M. 1981. Diffraction Physics, 2nd rev. ed. North-Holland Publishing, Amsterdam.

de Meis, L., and A. L. Vianna. 1979. Energy interconversion by the Ca^{2+}-dependent ATPase of the sarcoplasmic reticulum. *Annu. Rev. Biochem.* 48:275–292.

Ebashi, S., M. Endo, and I. Ohtsuki. 1969. Control of muscle contraction. *Q. Rev. Biophys.* 2:351–384.

Herbette, L., P. DeFoor, S. Fleischer, D. Pascolini, A. Scarpa, and J. K. Blasie. 1985. The separate profile structures of the functional calcium pump protein and the phospholipid bilayer within isolated sarcoplasmic reticulum membranes determined by x-ray and neutron diffraction. *Biochim. Biophys. Acta.* 817:103–122.

Herbette, L., J. Marquardt, A. Scarpa, and J. K. Blasie. 1977. A direct analysis of lamellar x-ray diffraction from hydrated oriented multilayers of fully functional sarcoplasmic reticulum. *Biophys. J.* 20:245–272.

Ikemoto, N. 1982. Structure and function of the calcium pump protein of sarcoplasmic reticulum. *Annu. Rev. Physiol.* 44:297–317.

Inesi, G. 1985. Mechanism of calcium transport. *Annu. Rev. Physiol.* 47:573–601.

Lesslauer, W., and J. K. Blasie. 1971. X-ray holographic interferometry in the determination of planar multilayer structures. Theory and experimental observations. *Acta Crystallogr.* A27:456–461.

Lowry, O. H., N. J. Rosebrough, A. L. Farr, and R. J. Randall. 1951. Protein measurement with the folin phenol reagent. *J. Biol. Chem.* 193:265–275.

MacLennan, D. H., C. J. Brandl, B. Korczak, and N. M. Green. 1985. Amino-acid sequence of a Ca^{2+} + Mg^{2+}-dependent ATPase from rabbit muscle sarcoplasmic reticulum, deduced from its complementary DNA sequence. *Nature.* 316:696–700.

Makowski, L. 1981. The use of continuous diffraction data as a phase constraint. I. One-dimensional theory. *J. Appl. Crystallogr.* 14:160–168.

McFarland, B. H., and G. Inesi. 1971. Solubilization of sarcoplasmic reticulum with Triton X-100. *Arch. Biochem. Biophys.* 145:456–464.

Meissner, G. 1975. Isolation and characterization of two types of sarcoplasmic reticulum vesicles. *Biochim. Biophys. Acta.* 389:51–68.

Meissner, G., G. E. Conner, and S. Fleischer. 1973. Isolation of sarcoplasmic reticulum by zonal centrifugation and purification of Ca^{2+}-pump and Ca^{2+}-binding proteins. *Biochim. Biophys. Acta.* 298:246–269.

Murphy, M. A., J. K. Blasie, L. J. Peticolas, and J. C. Bean. 1993. X-ray interferometry/holography for the unambiguous determination of the profile structures of single Langmuir-Blodgett monolayers. *Langmuir.* 9:1134–1141.

Pachence, J. M., and J. K. Blasie. 1991. Structural investigation of the covalent and electrostatic binding of yeast cytochrome *c* to the surface of various ultrathin lipid multilayers using x-ray diffraction. *Biophys. J.* 59:894–900.

Sagiv, J. 1980. Organized monolayers by adsorption. I. Formation and structure of oleophobic mixed monolayers on solid surfaces. *J. Am. Chem. Soc.* 102:92–98.

Skita, V., M. Filipkowski, A. F. Garito, and J. K. Blasie. 1986. Profile structures of very thin multilayers by X-ray diffraction using direct refinement methods of analysis. *Phys. Rev. B.* 34:5826–5837.

Smith, H. M. 1969. Principles of Holography. Wiley-Interscience, New York.

Squier, T. C., D. J. Bigelow, J. G. de Ancos, and G. Inesi. 1987. Localization of site-specific probes on the Ca-ATPase of sarcoplasmic reticulum using fluorescence energy transfer. *J. Biol. Chem.* 262:4748–4754.

Stroud, R. M., and D. A. Agard. 1979. Structure determination of asymmetric membrane profiles using an iterative Fourier method. *Biophys. J.* 25:495–512.

Toyoshima, C., H. Sasabe, and D. L. Stokes. 1993. Three-dimensional cryo-electron microscopy of the calcium ion pump in the sarcoplasmic reticulum membrane. *Nature.* 362:469–471.

Watras, J., F. C. Messineo, and L. G. Herbette. 1984. Mechanisms of fatty acid effects on sarcoplasmic reticulum. I. Calcium-fatty acid interaction. *J. Biol. Chem.* 259:1319–1324.

Xu, S., R. F. Fischetti, J. K. Blasie, L. J. Peticolas, and J. C. Bean. 1993. Profile and in-plane structures of self-assembled monolayers on Ge/Si multilayer substrates by high-resolution X-ray diffraction employing X-ray interferometry/holography. *J. Phys. Chem.* 97:1961–1969.

Xu, S., M. A. Murphy, S. M. Amador, and J. K. Blasie. 1991. Proof of asymmetry in the Cd-arachidate bilayers of ultrathin Langmuir-Blodgett multilayer films via x-ray interferometry. *J. Phys. I France.* 1:1131–1144.